LAWRENCE
LIVERMORE
NATIONAL
LABORATORY

LLNL-JRNL-610455

Use of spherical harmonics for dislocation dynamics in anisotropic elastic media

S. Aubry, A. Arsenlis

January 15, 2013

Modelling and Simulation in Materials Science and Engineering

Disclaimer

Use of spherical harmonics for dislocation dynamics in anisotropic elastic media

S. Aubry and A. Arsenlis

Lawrence Livermore National Laboratory, Livermore, CA, USA

Abstract

Large scale dislocation dynamics simulations usually involve several millions of interacting dislocation segments. The stress at a point and interaction force between two segments need to be computed many times during simulations. We evaluate the cost versus accuracy of using spherical harmonics series to approximate the anisotropic elastic Green's function in calculating stresses and forces between segments. The stress at a point is obtained by analytically integrating the spherical harmonics series once and the forces by integrating it analytically twice. We analyze the convergence and cost of using this approach and describe the elements of a fast implementation. We find that the cost of the force and stress calculations grows quadratically with the accuracy for a fixed anisotropy ratio.

Key words: Dislocations, anisotropic elasticity, dislocations interactions, spherical harmonics.

1 Introduction

Dislocation dynamics simulations often assume isotropic elasticity to compute stresses at points in the simulation volume and forces between dislocations. Anisotropic elasticity has been used to compute dislocation reactions and dynamics for a small dislocation ensembles like a dislocation loop, a Frank-Read source and two straight, interacting dislocations [1, 2, 3, 4, 5, 6]. For large, dense dislocation ensembles, anisotropic elasticity is rarely used due to its perceived computational cost. Most large scale simulations have resorted to using isotropic elastic approximations that are less computationally intensive.

It is difficult to bound the approximation that is made when using isotropic elasticity instead of anisotropic elasticity. Qualitative differences have been observed between isotropic and anisotropic media in the literature. For high

anisotropy, such as for α-iron at high temperature, it has been shown analytically [1], numerically [2] and experimentally [3] that prismatic and glide loops form sharp corners. These corners can only be captured when using the anisotropic elasticity formalism. It was also observed [4] that the critical stress to bow out a Frank-Read source is different when anisotropic elasticity is used compared to isotropic elasticity for the same material. This suggests that dislocation mechanisms can be significantly different when full anisotropy is considered. For a quantification of the error made using isotropic elasticity, M. Rhee *et al.* [5] have computed an error as high as 15% for Molybdenum which is moderately anisotropic ($A = 0.775$) for some components of the stress tensor in a hexagonal dislocation loop. Also, Han *et al.* [7] have concluded that the stress-strain behavior of copper ($A = 3.21$) cannot be reproduced using isotropic approximations.

The main reason anisotropic elasticity is not used in large scale dislocation dynamics simulations is its perceived cost. It has been shown that using the Willis-Steeds or the Brown formula [8] to compute interactions between dislocations in anisotropic elasticity can be orders of magnitude slower than the equivalent calculation in isotropic elasticity. The exact cost depends on the way forces between interacting dislocation segments are computed as well as the distance separating the segments [5, 7, 9]. The main difficulty in using anisotropic elasticity is that an analytical form of the anisotropic Green's function does not exist. The analytical form of the Green's function in isotropic elasticity has led to analytical expressions for the stress at a point and the force between two interacting segments [10]. Use of analytical forms enables a fast calculation of stresses and forces compared with numerical integration. Since an analytical definition of the Green's function is lacking in anisotropic elasticity, several attempts have be made to describe it efficiently. For instance, Rhee *et al.* [5] defined look-up tables to determine the angular part of the Green's function and its derivative. Unfortunately, these methods remain expensive and have seen a limited use in dislocation dynamics. They still require numerical integration of forces, and the accuracy and cost vary with relative distance between segments: the closer the interacting dislocation segments are, the more Gauss quadrature points are necessary to compute the forces between interacting pairs of segments accurately.

In this paper, we propose a fast implementation of dislocation interactions in anisotropic media that is practical for large scale simulations. The method is illustrated for the classical Volterra dislocation, using the singular theory recounted in Hirth and Lothe [8]. The key is to represent the Green's function with a spherical harmonics series. Mura *et al.* proposed this representation in 1971 [11]. The novelty is to observe that such a decomposition allows the single line integral involved in the definition of the stress at a point and the double line integral involved in the calculation of the forces to be expressed analytically once the coefficients of the series have been set. This alleviates

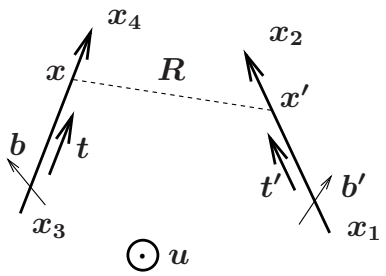

Fig. 1. Notations for two interacting segments: Dislocation segment $[\boldsymbol{x_1}, \boldsymbol{x_2}]$ with line direction $\boldsymbol{t'}$, length L' and Burgers vector $\boldsymbol{b'}$ and segment $[\boldsymbol{x_3}, \boldsymbol{x_4}]$ with line direction $\boldsymbol{t}$, Burgers vector $\boldsymbol{b}$ and length L. If $\boldsymbol{x}$ is a point on $[\boldsymbol{x_3}, \boldsymbol{x_4}]$ and $\boldsymbol{x'}$ a point on segment $[\boldsymbol{x_1}, \boldsymbol{x_2}]$, then $\boldsymbol{R} = \boldsymbol{x} - \boldsymbol{x'}$.

the need for numerical integration and drastically decreases the cost of stress and force evaluations.

Section 2 describes the expansion of the derivative of the Green's function into a spherical harmonics series and the integration procedure of that series leading to series expressions for the stress at a point due to a dislocation segment and the force between interacting segments. Section 3 shows how the integration of the spherical harmonics series can be computed in an efficient manner. Section 4 shows the numerical results for cost and accuracy of the proposed method. The last section compares our method to existing methods.

2 Stress and interactions forces in anisotropic elasticity

In dislocation dynamics simulations, dislocations are discretized into nodes connected by segments. The stress at a point due to a dislocation segment and the interaction force between a pair of segments can be defined using linear elasticity.

In a linear elastic domain, the stress at $\boldsymbol{x}$ due to a dislocation loop $\mathcal{C}$ with elastic stiffness tensor C_{ijkl} is given by Mura *et al.* 's formula [8]

$$\sigma_{js}(\boldsymbol{x}) = \epsilon_{ngr} C_{jsvg} C_{pqwn} b'_w \oint_{\mathcal{C}} \frac{\partial G_{vp}}{\partial x_q}(\boldsymbol{x} - \boldsymbol{x'}) dx'_r \tag{1}$$

where $\frac{\partial G_{vp}}{\partial x_q}$ is the first derivative of the Green's function, defined in more detail below, $\boldsymbol{b'}$ is the Burgers vector of the dislocation loop and $\boldsymbol{\epsilon}$ is the permutation tensor. The stress is determined uniquely when the integral is evaluated on a closed loop. This loop can be decomposed over a sum of straight segments to form a discretized polygonal loop.

In the dislocation dynamics code ParaDiS [10], forces are defined at the end

nodes of dislocation segments. There are a couple of equivalent ways to compute the force on a node of a discretized dislocation configuration. The force can be found as the minus derivative of the total energy with respect to the node position. Alternatively, the force on a node can be obtained using the virtual force argument i.e. by computing appropriate line integrals of the Peach-Koehler force over the segments connected to the node. Consider two segments $[\boldsymbol{x_1}, \boldsymbol{x_2}]$ and $[\boldsymbol{x_3}, \boldsymbol{x_4}]$ with Burgers vectors $\boldsymbol{b'}$ and $\boldsymbol{b}$ and lengths L' and L respectively, see Fig. 1 for notations. The contribution from segment $[\boldsymbol{x_1}, \boldsymbol{x_2}]$ to the force on node $\boldsymbol{x_4}$ is equal to the work of the Peach-Koehler force as the segment sweeps over a triangular shaped area due to a virtual displacement of node $\boldsymbol{x_4}$ [10] i.e.

$$\boldsymbol{F^4} = \int_{\boldsymbol{x_3}}^{\boldsymbol{x_4}} N(\boldsymbol{x}) \boldsymbol{\sigma^{12}}(\boldsymbol{x}) \cdot \boldsymbol{b} \times \boldsymbol{dx}$$

where N is the shape function $N(\boldsymbol{x}) = \frac{|\boldsymbol{x} - \boldsymbol{x_3}|}{|\boldsymbol{x_4} - \boldsymbol{x_3}|}$ where $\boldsymbol{x}$ is a point on segment $[\boldsymbol{x_3}, \boldsymbol{x_4}]$ and is defined such that it equals one when $\boldsymbol{x} = \boldsymbol{x_4}$ and zero when $\boldsymbol{x} = \boldsymbol{x_3}$.

When we evaluate the stress on a finite segment $[\boldsymbol{x_1}, \boldsymbol{x_2}]$, the force becomes a double line integral over the two dislocation segments,

$$F_i^4 = \epsilon_{ijo} \epsilon_{ngr} C_{jsvg} C_{pdwn} b_s b'_w \int_{\boldsymbol{x_1}}^{\boldsymbol{x_2}} \int_{\boldsymbol{x_3}}^{\boldsymbol{x_4}} \frac{\partial G_{vp}}{\partial x_d}(\boldsymbol{R}) \frac{|\boldsymbol{x} - \boldsymbol{x_3}|}{L} dx_o dx'_r \qquad (2)$$

where $\boldsymbol{R} = \boldsymbol{x} - \boldsymbol{x'}$ is the distance between two points $\boldsymbol{x}$ and $\boldsymbol{x'}$ belonging the two dislocation segments $[\boldsymbol{x_3}, \boldsymbol{x_4}]$ and $[\boldsymbol{x_1}, \boldsymbol{x_2}]$ respectively.

This latter definition of the force at a node Eq. (2) is convenient for force calculations as it explicitly gives the interaction force on the end nodes of the dislocation segments. Arsenlis *et al.* [10] showed that in isotropic elasticity, the force defined in Eq. (2) can be computed analytically thereby preventing expensive numerical integration.

2.1 Definition of the Green's function and its derivative

The stress and the interacting force between dislocations are defined through the Green's function. The Green's function $G_{kp}(\boldsymbol{x} - \boldsymbol{x'})$ is defined as the displacement in x_k-direction at point $\boldsymbol{x}$ in response to a unit point force in x_p-direction applied at point $\boldsymbol{x'}$. It is given explicitly in isotropic elasticity but not in anisotropic elasticity. The Green's function in anisotropic elasticity has

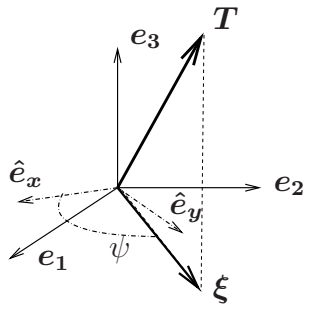

Fig. 2. Notations for the definition of the Green's function in anisotropic elasticity. The vector $\boldsymbol{T}$ is the unit vector $\boldsymbol{T} = \frac{\boldsymbol{R}}{R}$, ($\boldsymbol{e_1}$, $\boldsymbol{e_2}$, $\boldsymbol{e_3}$) is the basis where the elastic tensor C_{ijkl} is defined, ($\hat{\boldsymbol{e}}_{\boldsymbol{1}}$, $\hat{\boldsymbol{e}}_{\boldsymbol{2}}$) are two arbitrary unit vectors orthogonal to $\boldsymbol{T}$ and $\boldsymbol{\xi}$ is the projection of $\boldsymbol{T}$ onto ($\hat{\boldsymbol{e}}_{\boldsymbol{1}}$, $\hat{\boldsymbol{e}}_{\boldsymbol{2}}$) and makes an angle ψ with $\hat{\boldsymbol{e}}_{\boldsymbol{x}}$. By definition, $\boldsymbol{T} \cdot \boldsymbol{\xi} = 0$.

been described in detail by Bacon, Barnett and Scattergood [12] as

$$G_{kp} = \frac{1}{4\pi^2 R} \int_0^\pi M_{kp}^{-1}(\boldsymbol{\xi}) d\psi \tag{3}$$

where $\boldsymbol{M}^{-1}(\xi)$ is defined as

$$M_{kp}^{-1}(\xi) = \frac{\epsilon_{ksm}\epsilon_{prw}(\xi\xi)_{sr}(\xi\xi)_{mw}}{2\epsilon_{lgn}(\xi\xi)_{1l}(\xi\xi)_{2g}(\xi\xi)_{3n}}$$

where the notation $(\xi\xi)_{ij} = \xi_k C_{kijl} \xi_l$ is used. The matrix $\boldsymbol{M}^{-1}$ is a quotient of polynomials of order 4 in the numerator and 6 in the denominator. R is the norm of $\boldsymbol{R}$ and $\boldsymbol{T} = \frac{\boldsymbol{R}}{R}$ its direction. The vector $\boldsymbol{\xi}(\psi)$ is a unit vector for which $\boldsymbol{\xi} \cdot \boldsymbol{T} = 0$ and varies in the plane formed by ($\hat{\boldsymbol{e}}_{\boldsymbol{x}}$, $\hat{\boldsymbol{e}}_{\boldsymbol{y}}$) with an angle ψ. Vectors $\hat{\boldsymbol{e}}_{\boldsymbol{x}}$ and $\hat{\boldsymbol{e}}_{\boldsymbol{y}}$ are two arbitrary unit vectors defined in the plane orthogonal to $\boldsymbol{T}$, see Fig. (2) for notations. More details can be found in [12, 13]. A closed form analytical expression for the Green's function's integral does not exist.

The derivative of the Green's function is given in Barnett [13] as

$$\frac{\partial G_{kp}}{\partial x_q} = \frac{1}{4\pi^2 R^2} \int_0^\pi \left(-T_q M_{kp}^{-1} + \xi_q N_{kp} \right) d\psi$$

where

$$N_{kp} = C_{jrnw} M_{kj}^{-1} M_{np}^{-1} (\xi_r T_w + \xi_w T_r)$$

As defined the derivative of the Green's function is a product of a part depending only on $\frac{1}{R^2}$ and an angular part $\boldsymbol{g}$ depending only on the direction $\boldsymbol{T}$

$$g_{vpd}(\boldsymbol{T}) = g_{vpd}(\theta, \phi) = \int_0^\pi \left(-T_d M_{vp}^{-1} + \xi_d N_{vp} \right) d\psi \tag{4}$$

where $(\theta,\ \phi)$ are the spherical coordinates of $\boldsymbol{T}$, so that the derivative of the Green's function is

$$\frac{\partial G_{vp}}{\partial x_d}(\boldsymbol{R}) = \frac{g_{vpd}(\boldsymbol{T})}{4\pi^2 R^2}$$

There exists no analytical expression for g_{vpd}, however the function $g_{vpd}(\boldsymbol{T})$ is suitable for decomposition in spherical harmonics.

2.2 Decomposition in spherical harmonics

A continuous function $\boldsymbol{g}$ on the unit sphere can be expanded in a series of spherical harmonics

$$\boldsymbol{g}(\boldsymbol{T}) = \sum_{l=0}^{\infty} \sum_{m=-l}^{l} \boldsymbol{g}^{lm} Y_l^m(\boldsymbol{T}) \tag{5}$$

which uniformly converges on the unit sphere [11].

The expansion coefficients $\boldsymbol{g}^{lm}$ are independent of $\boldsymbol{T}(\theta,\phi)$ and are defined as

$$\boldsymbol{g}^{lm} = \int_0^{2\pi} \int_0^{\pi} \boldsymbol{g}(\theta,\phi) Y_l^{m*}(\theta,\phi)\ \sin\theta d\theta d\phi. \tag{6}$$

The spherical harmonics Y_l^m are defined as the complex functions

$$Y_l^m(\theta,\phi) = M_l^m P_l^m(\cos\theta) e^{im\phi}$$

where $M_l^m = \sqrt{\frac{(2l+1)}{4\pi}\frac{(l-m)!}{(l+m)!}}$ and P_l^m are the associated Legendre polynomials [14]. For any $m \in [-l, l]$, the spherical harmonics can be written explicitly as

$$Y_l^m(\theta,\phi) = (-1)^m M_l^{|m|} f_m(\phi) (\sin\theta)^{|m|} \sum_{k=0}^{[(l-|m|)/2]} \frac{(2l-2k)!}{2^l (l-k)!k!(l-2k-|m|)!} (-1)^k (\cos\theta)^{l-|m|-2k}$$

where we have posed

$$f_m(\phi) = \begin{cases} e^{im\phi} \text{ if } m \geq 0 \\ e^{-ip\phi} = \left[e^{ip\phi}\right]^* \text{ if } m < 0, m = -p \end{cases}$$

The spherical harmonics can be written in Cartesian coordinates in the basis $(\boldsymbol{e_1},\ \boldsymbol{e_2},\ \boldsymbol{e_3})$ where the coefficients C_{ijkl} are defined as a function of $x = \boldsymbol{T}\cdot\boldsymbol{e_1}$, $y = \boldsymbol{T}\cdot\boldsymbol{e_2}$ and $z = \boldsymbol{T}\cdot\boldsymbol{e_3}$ as

$$Y_l^m(\boldsymbol{T}) = (-1)^m M_l^{|m|} f_m(x,y) \sum_{k=0}^{[(l-|m|)/2]} \frac{(2l-2k)!}{2^l (l-k)!k!(l-2k-|m|)!} (-1)^k z^{l-|m|-2k} \tag{7}$$

with

$$f_m(x,y) = \begin{cases} (x+iy)^m \text{ if } m \geq 0 \\ (x-iy)^{-m} = \left[(x+iy)^{|m|}\right]^* \text{ if } m < 0 \end{cases}$$

All the factorials in Eq. (7) can be expressed using the binomial coefficients and rewritten in the form

$$Y_l^m(\boldsymbol{T}(x,y,z)) = f_m(x,y) \sum_{k=0}^{[(l-|m|)/2]} \bar{Q}_l^{|m|}(k) z^{l-|m|-2k} \tag{8}$$

where

$$\bar{Q}_l^m(k) = \frac{(-1)^{m+k}}{4\pi^2} \frac{m!}{2^l} \sqrt{\frac{(2l+1)}{4\pi} \frac{(l-m)!}{(l+m)!}} \binom{l}{k} \binom{2l-2k}{l} \binom{l-2k}{m} \tag{9}$$

The function $\boldsymbol{g}$ can be defined in terms of Eq. (8) and Eq. (9)

$$\boldsymbol{g}(x,y,z) = \sum_{l=0}^{\infty} \sum_{m=0}^{l} 2\Re\left((x+iy)^m \boldsymbol{g}^{lm}\right) \sum_{k=0}^{[(l-m)/2]} Q_l^m(k) z^{l-m-2k} \tag{10}$$

where we have noted $\Re(x)$ the real part of x and $Q_l^0(k) = \bar{Q}_l^0(k)$ when $m = 0$ and $Q_l^m(k) = 2\bar{Q}_l^m(k)$, when $m > 0$.

Applying the spherical harmonics series expansion to the angular part of the derivative on the Green's function and defining $x + iy = \frac{\boldsymbol{R}\cdot(\boldsymbol{e_1}+i\boldsymbol{e_2})}{R} \overset{\text{def}}{=} \frac{\boldsymbol{R}}{R} \cdot \boldsymbol{e_{12}}$ and $z = \frac{\boldsymbol{R}}{R} \cdot \boldsymbol{e_3}$

$$\frac{\partial G_{vp}}{\partial x_d}(\boldsymbol{R}) = \sum_{l=0}^{\infty} \sum_{m=0}^{l} \sum_{k=0}^{[(l-m)/2]} \Re\left(Q_l^m(k) g_{vpd}^{lm} \frac{(\boldsymbol{R}\cdot\boldsymbol{e_{12}})^m (\boldsymbol{R}\cdot\boldsymbol{e_3})^{l-m-2k}}{R^{l-2k+2}}\right)$$

This definition involves a quotient of terms that are a function of R which depends only on two variables m and $l - 2k$ and can be simplified further

$$\frac{\partial G_{vp}}{\partial x_d}(\boldsymbol{R}) = \sum_{q=0}^{\infty} \sum_{m=0}^{2q+1} \Re\left(S_{vpd}^{qm} \frac{(\boldsymbol{R}\cdot\boldsymbol{e_{12}})^m (\boldsymbol{R}\cdot\boldsymbol{e_3})^{2q+1-m}}{R^{2q+3}}\right) \tag{11}$$

where S_{vpd}^{qm} is a sum of products composed of $Q_l^m(k)$ and g_{vpd}^{lm}.

The Green's function and its derivative depend only on odd powers of $1/R$. This property means that in the expansion in spherical harmonics, the non-zero terms correspond to odd powers of $1/R$. For isotropic elasticity, the expansion in spherical harmonics is exact and only requires a truncated expansion up to $q = 1$.

Since the stress at a point, Eq. (1) and the force on an end node, Eq. (2) can be written as a function of the derivative of the Green' function, they can also be expanded in series using Eq. (11).

$$\sigma_{js}(\boldsymbol{x}) = \epsilon_{ngr} C_{jsvg} C_{pdwn} b'_w \sum_{q=0}^{\infty} \sum_{m=0}^{2q+1} \Re \left(S_{vpd}^{qm} \int_{\boldsymbol{x_1}}^{\boldsymbol{x_2}} \frac{(\boldsymbol{R}\cdot\boldsymbol{e_{12}})^m (\boldsymbol{R}\cdot\boldsymbol{e_3})^{2q+1-m}}{R^{2q+3}} \, dx'_r \right) \tag{12}$$

and

$$F_i^4 = \epsilon_{ijo}\epsilon_{ngr} C_{jsvg} C_{pdwn} b_s b'_w \sum_{q=0}^{\infty} \sum_{m=0}^{2q+1} \Re \left(S_{vpd}^{qm} \int_{\boldsymbol{x_1}}^{\boldsymbol{x_2}} \int_{\boldsymbol{x_3}}^{\boldsymbol{x_4}} \frac{(\boldsymbol{R}\cdot\boldsymbol{e_{12}})^m (\boldsymbol{R}\cdot\boldsymbol{e_3})^{2q+1-m}}{R^{2q+3}} \frac{|\boldsymbol{x}-\boldsymbol{x_3}|}{L} dx_o dx'_r \right) \tag{13}$$

These equations for the stress and the force reveal single and double integrals over the dislocation segments. The advantage of writing the stress and the force using expansion in spherical harmonics series is the possibility to derive efficiently via recurrence these integrals analytically. The calculations of the single line integral

$$J_{ijp}(\boldsymbol{R}) = \int \frac{(\boldsymbol{R}\cdot\boldsymbol{e_3})^i (\boldsymbol{R}\cdot\boldsymbol{e_{12}})^j}{R^p} ds \tag{14}$$

and the double line integral

$$H_{ijp}(\boldsymbol{R}) = \int\int \frac{(\boldsymbol{R}\cdot\boldsymbol{e_3})^i (\boldsymbol{R}\cdot\boldsymbol{e_{12}})^j}{R^p} dr ds \tag{15}$$

using recurrence relations are given in the Appendix. Following the definition of the stress and the force, the powers i, j and p are linked by the relation $i + j = p - 2$ which limits the number of integrals to compute. Furthermore, p is odd and $p \geq 3$.

Section A.1 of the appendix gives the recurrence relations for the force in the case of two non-parallel, non-intersecting segments. Section A.2 of the appendix gives the recurrence relations in the case of two parallel, non-intersecting segments. Section A.3 gives the recurrence relations in the case of two collinear, non intersecting segments. Section A.4 gives the recurrence relations for the stress at a point whether the point is collinear to the segment or not.

3 Implementation of anisotropic elastic stress and force

Several elements in the force and stress formula can be pre-computed independently of the dislocation segments for faster calculation.

The product S_{vpd}^{qm} is a function of expansion coefficients g_{vpd}^{lm}. It does not depend on the exact geometry of the interacting pair of segments and can be pre-computed once at the beginning of the simulation.

The $3 \times 3 \times 3 \times 3$ stiffness tensor C_{ijlk} is often written in a contracted matrix notation $C_{\alpha\beta}$, a 6×6 matrix, to take advantage of symmetry in the strain definition. For instance, a 3×3 tensor A can be written as a 6 dimensional vector A

$$\begin{cases} A_1 = \mathrm{A}_{11} \\ A_2 = \mathrm{A}_{22} \\ A_3 = \mathrm{A}_{33} \\ A_4 = \mathrm{A}_{12} + \mathrm{A}_{21} \\ A_5 = \mathrm{A}_{23} + \mathrm{A}_{23} \\ A_6 = \mathrm{A}_{13} + \mathrm{A}_{31} \end{cases} \tag{16}$$

and we can define an operator o such that $A_\alpha = \mathrm{o}_\alpha^{ij}[\mathrm{A}_{ij}]$ by the transformation defined in Eqs 16 where α varies in $\{1, 6\}$ and (i, j) in $\{1, 3\}$.

Using symmetries, the series expansion of the stress Eq. (12) can be simplified. The $3 \times 3 \times 3$ matrix

$$\mathrm{I}_{vpd} = \sum_{q=0}^{\infty} \sum_{m=0}^{2q+1} \Re \left(S_{vpd}^{qm} \int_0^{L'} \frac{(\boldsymbol{R} \cdot \boldsymbol{e_{12}})^m (\boldsymbol{R} \cdot \boldsymbol{e_3})^{2q+1-m}}{R^{2q+3}} \, d\xi_r' \right)$$

can be contracted into a 3×6 matrix, $I_{v\alpha} = o_\alpha^{pd}[\mathrm{I}_{vpd}]$. In the definition of the integral, the change of variable $\boldsymbol{x'} = (1 - \frac{\xi'}{L'})\boldsymbol{x_1} + \frac{\xi'}{L'}\boldsymbol{x_2}$ has been made.

The $3 \times 3 \times 3$ matrix **B'** defined as

$$\mathrm{B}'_{pdg} = \sum_{w,n,r} C_{pdwn} \epsilon_{ngr} b'_w t'_r$$

can also be contracted as a 6×3 matrix noted $B'_{\alpha g} = o_\alpha^{pd}[\mathrm{B'}_{pdg}]$. Using the definitions of **I** and **B'**, the stress becomes

$$\sigma_{js}(\boldsymbol{x}) = C_{jsvg} \mathrm{B}'_{pdg} \mathrm{I}_{vpd}$$

and the contracted form of the stress at a point $\sigma_\gamma(\boldsymbol{x})$ from Eq. (12) can be

written

$$\sigma_\gamma(\boldsymbol{x}) = C_{\gamma\beta}\, o_\beta^{vg}[IB']$$

Similarly, the expression Eq. (13) for the force can also be simplified. The $3 \times 3 \times 3$ matrix

$$\mathrm{O}_{vpd} = \sum_{q=0}^{\infty} \sum_{m=0}^{2q+1} \Re \left(S_{vpd}^{qm} \int_0^L \int_0^{L'} \frac{(\boldsymbol{R}\cdot\boldsymbol{e_{12}})^m (\boldsymbol{R}\cdot\boldsymbol{e_3})^{2q+1-m}}{R^{2q+3}} \frac{\xi}{L}\, d\xi d\xi' \right)$$

can be contracted into a 3×6 matrix, $O_{v\alpha} = o_\alpha^{pd}[\mathrm{O}_{vpd}]$. In the definition of the integrals, the changes of variable $\boldsymbol{x} = (1 - \frac{\xi}{L})\boldsymbol{x_3} + \frac{\xi}{L}\boldsymbol{x_4}$ and $\boldsymbol{x'} = (1 - \frac{\xi'}{L'})\boldsymbol{x_1} + \frac{\xi'}{L'}\boldsymbol{x_2}$ have been made.

The $3 \times 3 \times 3$ matrix $\mathbf{A}$ whose components are

$$\mathrm{A}_{ivg} = \sum_{j,s,o} C_{jsvg}\epsilon_{ijo} b_s t_o$$

can also be contracted as 3×6 matrix $A_{i\beta} = o_\beta^{vg}[\mathrm{A}_{ivg}]$.

Using the three matrices **A**, **B'** and **O**, the force becomes

$$F_i^4 = \mathrm{A}_{ivg}\mathrm{B}'_{\mathrm{pdg}}\mathrm{O}_{\mathrm{vpd}}$$

and the contracted form of the force from Eq. (13) can be written

$$F_i^4 = A_{i\beta}\, o_\beta^{vg}[OB']$$

4 Numerical results

The expansion of the force in spherical harmonics series in Eq. (13) depends on expansion coefficients g_{vpd}^{lm}, defined in Eq. (6) and on the integrals H_{ijk}, defined in Eq. (15). The expansion coefficients g_{vpd}^{lm} are defined as a double integral over angles (θ, ϕ) of the function $\boldsymbol{g}(\theta, \phi)$, Eq. (6). For a fixed couple of angles (θ, ϕ) or direction $\boldsymbol{T}$, the function $\boldsymbol{g}(\boldsymbol{T})$ is also defined as an integral over an angle ψ as shown by Eq. (4).

For a given direction $\boldsymbol{T}$, evaluating the function g involves a numerical integration over $\psi \in [0, \pi]$. The number of angles ψ needed to describe this integral is shown in Fig. (3)[a]. The error in calculating the $\boldsymbol{g}$ at a point on the sphere varies as a function of the number of angles chosen to discretize the integral. Approximately 100 angles are sufficient to obtain machine precision accuracy for a material with an anisotropy less than 8.

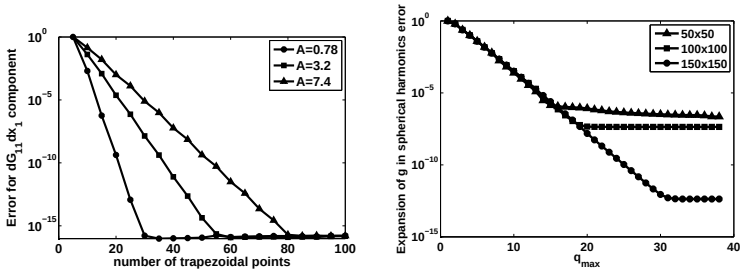

(a) Integral convergence (b) Grid convergence

Fig. 3. (a) Convergence of the integral defining the angular part of the derivative of the Green's function, Eq. (4). 100 points are sufficient to represent the integral with machine precision. (b) Convergence of the number of points to discretize the angles (θ, ϕ) to represent the angular part of the derivative of the Green's function correctly using spherical harmonics series, Eq. (5). 150×150 grid describes the derivative of the Green's function with an accuracy of 10^{-13}.

The expansion coefficients g_{vpd}^{lm} in Eq. (6) are defined as the double integral over the angles (θ, ϕ) of the product of the angular part of derivative of the Green's function $\boldsymbol{g}$ and the conjugate of the spherical harmonics Y_l^{*m}. The function $\boldsymbol{g}(\theta, \phi)$ is evaluated by the method above at discrete grid points on the unit sphere into a grid where the angles $\theta \in [0, \pi]$ and $\phi \in [0, 2\pi]$ are discretized. For each pair of angles, the integral in Eq. (5) is computed numerically as described in the previous paragraph. The double integral in Eq. (6) over ϕ is computed using the trapezoidal rule, and the integral over θ is computed using Gauss quadrature to obtain the expansion coefficients. The accuracy of the calculations for the expansion coefficients g_{vpd}^{lm} depends on the number of grid points chosen for discretizing the function on the unit sphere. Fig. 3[b] shows how the error between computing g in Eq. (4) and its expansion in spherical harmonics in Eq. (5) varies as a function of the number of angles (θ, ϕ) chosen. For about 150×150 grid points, 13 decimal places can be achieved.

In application, the spherical harmonics series used to describe the stress (Eq. 12) or the force (Eq. 13) must be truncated. The truncation number is noted $q_{\max}$. The larger the expansion order $q_{\max}$ considered in the series the more accurate and more expensive the calculations of the stress and the force calculations become. For instance, if the material is isotropic, i.e. has a coefficient of anisotropy

$$A = \frac{2C_{44}}{C_{11} - C_{22}}$$

of 1 then truncating the series at $q_{\max} = 1$ gives the exact solution. For all the anisotropic ratios, the solution becomes approximate but fully precise.

The error in the force calculation is evaluated by computing how much accuracy is gained by adding a new term in the spherical harmonics series. This error is defined as the average between the relative error on the four norms

of the force on the four nodes of two interacting orthogonal segments, each of length $L = 100$ and separated by a distance of $d = 10$ in arbitrary units. The error is computed such that

$$\delta F_{\text{error}}(q) = \frac{1}{4}\sum_{i=1}^{4}\frac{|F_i^q - F_i^{q+1}|}{|F_i^q|}$$

The main cost of the interaction force or stress calculations resides in the calculations of the integrals J, H (see Eqs. (14-15)) as everything else can either be pre-computed independently of the two segments lengths and directions or computed efficiently using the contracted matrices $\boldsymbol{A}$ and $\boldsymbol{B'}$ as defined in section 3. Fig. 4[a] shows the time spent in computing forces as $q_{\max}$ increases. That cost is computed as the time spent to compute force for a particular $q_{\max}$ versus the time spent to compute the same forces using isotropic elasticity i.e. $q_{\max} = 1$. The polynomial fit of Fig. 4[a] shows that this cost is quadratic in $q_{\max}$.

The expansion order $q_{\max}$ needed to compute forces accurately is related to the anisotropy of the elastic media. As the anisotropy increases, more coefficients in the spherical harmonics series are needed to reach a given accuracy. Fig. 4[b] shows how the error in force calculations varies as a function of increasing anisotropy A and cost. This cost in turn is related to $q_{\max}$. For $A = 1$, the isotropic case, the error in the force calculations is 10^{-16} for $q_{\max} = 1$. For $A = 7.4$, corresponding to $\alpha-$Fe at 900^oC, an error of 3×10^{-6} is reached for $q_{\max} = 20$ and is 56 times more expensive than isotropic elasticity.

Fig. 5[a] shows how the error in force calculations decreases with the expansion order $q_{\max}$ in the spherical harmonics series for a few values of anisotropy ratio A. This decrease is linear. The convergence rate can be fitted as a function of $\log A$. Fig. 5[b] shows a numerical fit of the form $-\exp[-(\alpha \log A + \beta)^\gamma]$. Parameters α, β and γ differ slightly between the right and the left fit of the data and are given by $\alpha = 0.82$ and -0.87, $\beta = -0.04$ and 0.01 and $\gamma = 2.2$ and 1.6 for the left and right fits respectively. In summary, the log of the error in force calculations varies as $-\exp[-(\alpha \log A + \beta)^\gamma] q_{\max}$ where A is the anisotropy ratio and $q_{\max}$ the expansion order.

The convergence of the spherical harmonics series also depends on the geometry of the two interacting segments. We consider the same two non-parallel segments as before but now we vary the distance d between the two segments. The error made by computing the interaction forces as a function of distance d/L is shown in Fig. 6 for three different anisotropic coefficients of 1.0, 3.7 and 7.4 going from no, intermediate to large anisotropy. The error in force calculations does not strongly depend on the distance between the two segments.

The cost and accuracy for the calculation of a stress at a point, Eq. 12 as

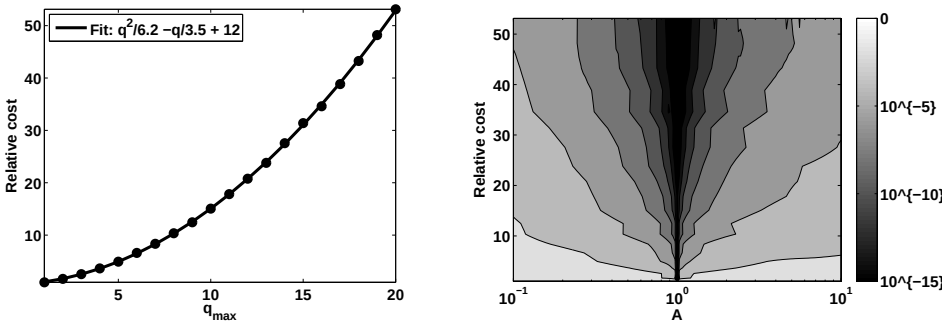

(a) Cost (b)

Fig. 4. (a) Cost relative to isotropic calculations of computing interaction forces between two non-parallel segments of length $L = 100$ and separated by a distance $d = 10$ as the expansion order $q_{\max}$ in the spherical harmonics series increases. A polynomial fit shows that the cost grows quadratically as a function of $q_{\max}$. (b) Error in the force calculation as a function of cost and anisotropy.

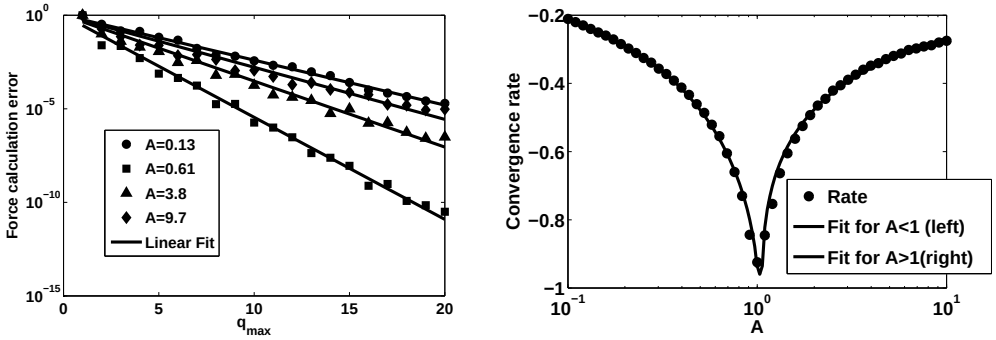

(a) (b)

Fig. 5. (a) The error in force calculation decreases linearly with $q_{\max}$ and is shown for a few values of anisotropy A for clarity. A linear fit is also shown for each curve. (b) The convergence rate observed in (a) can be fitted by a function of the form $-\exp[-(\alpha \log A + \beta)^{\gamma}]$, see values of α, β and γ in the text.

$q_{\max}$ and A increases have also been analyzed. The same qualitative behavior exhibited by the interaction force between two segments is observed for the computation of the stress at a point on one segment coming from the other segment.

5 Discussions and conclusion

Dislocation dynamics (DD) simulations involve heavy calculations. To account for hardening and dislocation patterning and avoid small volume artifacts, DD simulations require several millions of dislocation segments and millions of steps to reach the strain levels at which the hardening transitions are observed

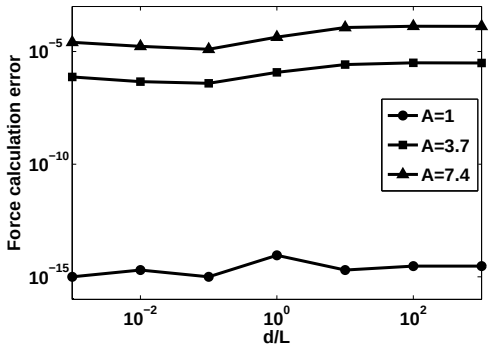

Fig. 6. Convergence of the error in force calculations as a function of the distance d separating the two interacting segments of fixed length $L = 100$ for two anisotropic ratio. The error in force calculations remains stationary with increasing relative distance between the two dislocation segments.

in isotropic elasticity i.e. $1-2$ percent of strain [15]. At each step, dislocations segment-segment interactions are computed analytically when the segments are close to each other and using the fast multipole method when they are far away [10]. The interaction force between two segments or the stress between a point and a segment calculations are the most repeated and expensive parts of a DD simulation.

The interaction force between two dislocation segments in anisotropic elasticity has been computed using either the Brown or the Willis-Steeds formalisms in previous works [5, 9]. Using these methods, the stress is integrated numerically at Gauss quadrature points on the dislocation segments and then summed up to get the force at the end nodes of the two segments. This method performs better when the two segments are far apart. As the segments get close to each other, more integration points are necessary to retain the accuracy of the force. Numerically integrating over segments has been found to be expensive in DD simulations. Rhee *et al.* [5] report that this method is 500 times more expensive than the equivalent calculation in isotropic elasticity. Yin *et al.* [9] have been able to reduce the cost and reported a cost of 220 for using anisotropic elasticity versus isotropic elasticity for tungsten. The variability of the costs reported is not surprising given that Arsenlis *et al.* [10] showed that the cost of numerical integration could vary by orders of magnitude depending on the separation of the line segments in isotropic elasticity.

Using an expansion in spherical harmonics series for the Green's function allows for analytical integration over a segment for the stress at a point and over two segments for the force. The accuracy of this decomposition does not depend on how many integration points are chosen to evaluate integrals but rather on the order of truncation in the spherical harmonics series which can be chosen to specify a predetermined accuracy for a given level of elastic anisotropy. Analytical integration overcomes deterioration of accuracy of the

calculations as the segments get closer.

In isotropic elasticity, an analytical expression to compute the forces between interacting pairs of segments is given in Arsenlis *et al.* [10]. A calculation of the number of operations between analytically computing forces in isotropic, as defined in [10], and anisotropic elasticity using spherical harmonics series shows that there are about 850 multiplications, 600 additions and subtractions and about 60 other operations like logs, square roots, divisions and arc tangents for isotropic elasticity versus about 2450 multiplications, 1300 additions and subtractions and 40 other operations in anisotropic elasticity for $q_{\max} = 1$. Since cost comparisons between two different codes can vary significantly with different compilers, if we were to estimate a cost similar to the previously reported in the literature, for our new method, we could amplify the relative cost reported in Fig. (4)[a] by a factor $1.5 - 3$.

As explained in Arsenlis *et al.* [10], the cost of computing interaction forces is balanced out between near and far field interactions in a DD simulation. A typical DD simulation domain is decomposed in cells. For two cells in the simulation domain, the interaction force between dislocations within those cells is computed either by using direct calculation of the forces or using the fast multipole method. The distance between two cells determines which method is used. Local interactions scale as $\mathcal{O}(n^2)$ and far away interactions scale as $\mathcal{O}(N)$ where N is total number of segments in the simulation and n is the number of segments per cell. An optimal choice of the number of cells and the ratio of n/N can be computed to decrease the cost of local anisotropic calculations. Assuming that the cost of the fast multipole method is comparable between isotropic and anisotropic elasticity, then the total cost of the calculation would increase by the square root of the cost factors discussed because the fraction of near field to far field would be rebalanced to optimize the total force calculation.

The convergence of the error in the force calculations decreases linearly with the expansion order $q_{\max}$ in the spherical harmonics series. As $q_{\max}$ increases, the terms in the coefficients $Q_l^m(k)$ grow quickly. When using double precision to store numbers, a lack of precision in the calculations starts to appear for $q_{\max} > 21 - 25$. This instability is due to the explicit description of the associated Legendre polynomials into a product of $\boldsymbol{S}$ and H. Nevertheless, in our simulations, $q_{\max} = 21$ corresponds to an accuracy in force calculations that does not exceed 10^{-4}. Fig. (7) shows the error in force calculation when $q_{\max}$ is fixed to 21. In practice, $q_{\max}$ may not go beyond 10 or so. One way to improve the limitation in the expansion order in the spherical harmonics would be to increase the rate of convergence of the error. For instance, polynomials other than Legendre may converge faster with increasing expansion order.

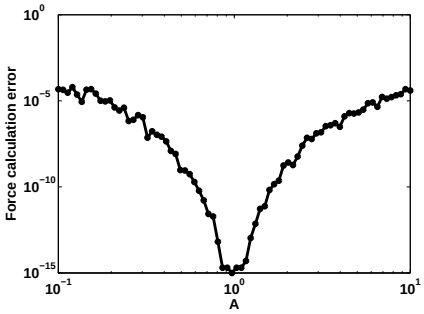

Fig. 7. Force calculation error between two non-parallel segments of length $L = 100$ and separated by a distance $d = 10$ as the expansion order $q_{\max}$ in the spherical harmonics series is set to 21. The error in force calculation does not exceed 10^{-4}.

A Appendix

The following sections describe how to determine the double line integral involved in the computation of the force in the case of two collinear, parallel and non-parallel dislocation segments. The single integral for computing the stress at a point coming from a dislocation segment is determined in the case where the point is collinear to the segment or not.

A.1 Recurrence relations for two non-parallel segments

The interaction force, Eq. (13) between two non-parallel, non-intersecting and non-collinear dislocation segments $[\boldsymbol{x_3}, \boldsymbol{x_4}]$ and $[\boldsymbol{x_1}, \boldsymbol{x_2}]$ with line directions $\boldsymbol{t}$ and $\boldsymbol{t'}$ and lengths L and L' respectively is

$$F_i^4 \approx \epsilon_{ijo}\epsilon_{ngr}C_{jsvg}C_{pdwn}b_s b'_w t_o t'_r \sum_{q=0}^{q_{\max}} \sum_{m=0}^{2q+1} \Re\left(\frac{S_{vpd}^{qm}}{L}[H^s_{m,(2q+1-m),2q+3} - s_3 H_{m,(2q+1-m),2q+3}]\right)$$

when it is expressed using the double line integral

$$\begin{aligned} H^s_{ijk} &= \int_{s_1}^{s_2}\int_{r_1}^{r_2} \frac{(\boldsymbol{R}\cdot\boldsymbol{e_{12}})^i(\boldsymbol{R}\cdot\boldsymbol{e_3})^j}{R^k} s ds dr \\ H_{ijk} &= \int_{s_1}^{s_2}\int_{r_1}^{r_2} \frac{(\boldsymbol{R}\cdot\boldsymbol{e_{12}})^i(\boldsymbol{R}\cdot\boldsymbol{e_3})^j}{R^k} ds dr \end{aligned} \tag{A.1}$$

where $i + j = k - 2$ and k is odd.

If the force is evaluated on the end nodes $\boldsymbol{x_1}$ or $\boldsymbol{x_2}$ instead of $\boldsymbol{x_4}$, the double integral

$$H^r_{ijk} = \int_{s_1}^{s_2}\int_{r_1}^{r_2} \frac{(\boldsymbol{R}\cdot\boldsymbol{e_{12}})^i(\boldsymbol{R}\cdot\boldsymbol{e_3})^j}{R^k} r ds dr$$

is used instead of H^s.

$\boldsymbol{R}$ is the distance between the two dislocation segments and R is the norm of $\boldsymbol{R}$. It can be defined as $\boldsymbol{R} = s\boldsymbol{t} + r\boldsymbol{t'} + d\boldsymbol{u}$ where

$$s = \frac{\boldsymbol{R}\cdot\boldsymbol{t} - c\boldsymbol{R}\cdot\boldsymbol{t'}}{1-c^2} \qquad r = \frac{\boldsymbol{R}\cdot\boldsymbol{t'} - c\boldsymbol{R}\cdot\boldsymbol{t}}{1-c^2}$$
$$\boldsymbol{u} = \boldsymbol{t}\times\boldsymbol{t'} \qquad d = \frac{(\boldsymbol{x_3}-\boldsymbol{x_1})\cdot\boldsymbol{u}}{\boldsymbol{u}\cdot\boldsymbol{u}} \qquad c = \boldsymbol{t}\cdot\boldsymbol{t'}$$

Variables s and r vary in the intervals $[s_3,\ s_4]$ and $[r_1,\ r_2]$ respectively where

$$r_1 = \frac{(\boldsymbol{x_3}-\boldsymbol{x_1})\cdot\boldsymbol{v'}}{\boldsymbol{u}\cdot\boldsymbol{u}} \qquad s_3 = \frac{(\boldsymbol{x_3}-\boldsymbol{x_1})\cdot\boldsymbol{v}}{\boldsymbol{u}\cdot\boldsymbol{u}}$$

where we have posed $\boldsymbol{v} = \boldsymbol{t'} - c\boldsymbol{t}$ and $\boldsymbol{v'} = \boldsymbol{t} - c\boldsymbol{t'}$.

Finally, we define α, β, γ, δ, ϵ and θ as follows

$$\boldsymbol{R}\cdot\boldsymbol{e_{12}} = s\,\boldsymbol{t}\cdot\boldsymbol{e_{12}} + r\,\boldsymbol{t'}\cdot\boldsymbol{e_{12}} + d\,\boldsymbol{u}\cdot\boldsymbol{e_{12}} \stackrel{\text{def}}{=} s\alpha + r\beta + \gamma$$
$$\boldsymbol{R}\cdot\boldsymbol{e_3} = s\,\boldsymbol{t}\cdot\boldsymbol{e_3} + r\,\boldsymbol{t'}\cdot\boldsymbol{e_3} + d\,\boldsymbol{u}\cdot\boldsymbol{e_3} \stackrel{\text{def}}{=} s\delta + r\epsilon + \theta$$

and we pose $K_{ijk} = \frac{(\boldsymbol{R}\cdot\boldsymbol{e_{12}})^i(\boldsymbol{R}\cdot\boldsymbol{e_3})^j}{R^k}$.

A.1.1 Calculations of single integrals J^s and J^r

The single integrals

$$J^s_{ijk} = \int K_{ijk}ds$$
$$J^r_{ijk} = \int K_{ijk}dr \tag{A.2}$$

can be computed via recurrence.

The initial terms of J^r to start the recurrence are $J^r_{(-1)jk} = J^r_{i(-1)k} = 0$ and

$$\begin{aligned} J^r_{001} &= \ln(R + \boldsymbol{R}\cdot\boldsymbol{t'}) \\ J^r_{101} &= \beta R + ((\alpha - c\beta)s + \gamma)J^r_{001} \\ J^r_{011} &= \epsilon R + ((\delta - c\epsilon)s + \theta)J^r_{001}. \end{aligned} \tag{A.3}$$

The higher order terms are

$$J^r_{ij(k+2)} = \frac{1}{k(1-c^2)(d^2+s^2)}\Big[(k-i-j-1)J^r_{ijk} + (\boldsymbol{R}\cdot\boldsymbol{t'})K_{ijk} + i((\alpha-c\beta)s+\gamma)J^r_{(i-1)jk} + j((\delta-c\epsilon)s+\theta)J^r_{i(j-1)k}\Big] \quad \text{(A.4)}$$

$$J^r_{i(j+1)(k+2)} = \frac{\epsilon}{k}\Big[i\beta J^r_{(i-1)jk} + j\epsilon J^r_{i(j-1)k} - K_{ijk}\Big] + ((\delta-c\epsilon)r+\theta)J^r_{ij(k+2)}$$

$$J^r_{(i+1)j(k+2)} = \frac{\beta}{k}\Big[j\epsilon J^r_{i(j-1)k} + i\beta J^r_{(i-1)jk} - K_{ijk}\Big] + ((\alpha-c\beta)s+\gamma)J^r_{ij(k+2)}$$

The line integral J^s is defined by similar recurrence relations. They are deduced from the definition of Eqs. (A.3-A.4) by replacing r by s, δ by α, ϵ by β, θ by γ and $\boldsymbol{t'}$ by $\boldsymbol{t}$.

A.1.2 Recurrence for H^s, H^r and H

The double integrals H^s, H^r and H can also be defined using recurrence relations that are functions of the recurrence relations for the single line integrals J^s and J^r.

Initial terms to start the recurrence are $H_{(-1)jk} = H_{i(-1)k} = H^s_{(-1)jk} = H^s_{i(-1)k} = H^r_{(-1)jk} = H^r_{i(-1)k} = 0$ and

$$H_{003} = -\frac{2}{|\boldsymbol{R}\cdot\boldsymbol{u}|}\tan^{-1}\left(\frac{(1+c)R + \boldsymbol{R}\cdot(\boldsymbol{t}+\boldsymbol{t'})}{|\boldsymbol{R}\cdot\boldsymbol{u}|}\right)$$

If we define

$$I_{203} = rJ^s_{001} + \frac{cR - d^2(1-c^2)H_{003}}{1-c^2}$$
$$I_{023} = sJ^r_{001} + \frac{cR - d^2(1-c^2)H_{003}}{1-c^2}$$
$$I_{113} = -\frac{R - cd^2(1-c^2)H_{003}}{1-c^2}$$

then low order terms for H^s and H^r are

$$H^s_{103} = \alpha I_{203} + \beta I_{113} + \gamma H^s_{003}$$
$$H^s_{013} = \delta I_{203} + \epsilon I_{113} + \theta H^s_{003}$$
$$H^r_{103} = \alpha I_{113} + \beta I_{023} + \gamma H^r_{003} \quad \text{(A.5)}$$
$$H^r_{013} = \delta I_{113} + \epsilon I_{023} + \theta H^r_{003}. \quad \text{(A.6)}$$

Higher order terms are

$$
\begin{aligned}
H^s_{ij(k+2)} &= \frac{1}{k(1-c^2)}\left[i(\alpha-c\beta)H_{(i-1)jk} + j(\delta-c\epsilon)H_{i(j-1)k} - J^r_{ijk} + cJ^s_{ijk}\right] \\
H^r_{ij(k+2)} &= \frac{1}{k(1-c^2)}\left[i(\beta-c\alpha)H_{(i-1)jk} + j(\epsilon-c\delta)H_{i(j-1)k} - J^s_{ijk} + cJ^r_{ijk}\right] \\
H_{ij(k+2)} &= \frac{1}{k(1-c^2)d^2}\left[sJ^r_{ijk} + rJ^s_{ijk} + i\gamma H_{(i-1)jk} + j\theta H_{i(j-1)k} - (2+i+j-k)H_{ijk}\right] \\
H_{(i+1)jk} &= \alpha H^s_{ijk} + \beta H^r_{ijk} + \gamma H_{ijk} \\
H_{i(j+1)k} &= \delta H^s_{ijk} + \epsilon H^r_{ijk} + \theta H_{ijk}
\end{aligned}
\tag{A.7}
$$

When the dislocation segments are parallel, $c = 1$. The recurrence relations J^s and J^r, Eqs. (A.3-A.4), remain valid but the ones defining H, H^s and H^r, Eqs. (A.6-A.7) are not well defined anymore. Recurrences specific to parallel segments are given in the next section.

A.2 Recurrence relations for two parallel segments

When two dislocation segments are parallel but not collinear and assuming without loss of generality that their line direction is $\boldsymbol{t}$, their distance is $\boldsymbol{R} = (s+r)\boldsymbol{t} + d\boldsymbol{u}$ where now

$$
\boldsymbol{u} = \boldsymbol{R} - (\boldsymbol{R}\cdot\boldsymbol{t})\boldsymbol{t} \qquad\qquad d = \frac{\boldsymbol{R}\cdot\boldsymbol{u}}{\boldsymbol{u}\cdot\boldsymbol{u}}.
$$

We pose $\alpha = \boldsymbol{t}\cdot\boldsymbol{e_{12}}$, $\gamma = d\boldsymbol{u}\cdot\boldsymbol{e_{12}}$, $\delta = \boldsymbol{t}\cdot\boldsymbol{e_3}$ and $\theta = d\boldsymbol{u}\cdot\boldsymbol{e_3}$.

The initial terms to start the recurrence are

$$
\begin{aligned}
H_{003} &= \frac{R}{d^2(1-c^2)} \\
H^s_{003} &= -\frac{1}{2}\left[J^s_{001} + \frac{(s-r)}{d^2(1-c^2)}R\right] \\
H^r_{003} &= -\frac{1}{2}\left[J^s_{001} + \frac{(r-s)}{d^2(1-c^2)}R\right]
\end{aligned}
$$

and also

$$
\begin{aligned}
I_{203} &= rJ^s_{001} - R \\
I_{023} &= sJ^r_{001} - R
\end{aligned}
$$

Low order terms for H^s and H^r are

$$\begin{aligned}
H^s_{103} &= \alpha I_{203} + \gamma H^s_{003} \\
H^s_{013} &= \delta I_{203} + \theta H^s_{003} \\
H^r_{103} &= \alpha I_{023} + \gamma H^r_{003} \\
H^r_{013} &= \delta I_{023} + \theta H^r_{003}
\end{aligned}$$

The higher order terms are

$$\begin{aligned}
H^s_{ij(k+2)} =& \frac{1}{kd^2(1-c^2)}\Big[(k-i-j-2)H^s_{ijk} - H^r_{ijk} + i\gamma H^s_{(i-1)jk} + j\theta H^s_{i(j-1)k} + \\
& \frac{s}{k-2}\Big(i\alpha J^s_{(i-1)j(k-2)} + j\delta J^s_{i(j-1)(k-2)} - k(\boldsymbol{R}\cdot\boldsymbol{t})K_{ijk}\Big)\Big] \\
H^r_{ij(k+2)} =& \frac{1}{kd^2(1-c^2)}\Big[(k-i-j-2)H^r_{ijk} - H^s_{ijk} + i\gamma H^r_{(i-1)jk} + j\theta H^r_{i(j-1)k} + \\
& \frac{r}{k-2}\Big(i\alpha J^s_{(i-1)j(k-2)} + j\delta J^s_{i(j-1)(k-2)} - k(\boldsymbol{R}\cdot\boldsymbol{t})K_{ijk}\Big)\Big] \\
H^s_{i(j+1)(k+2)} =& \frac{\delta}{k}\Big[H_{ijk} + j\delta H^s_{i(j-1)k} + i\alpha H^s_{(i-1)jk} - sJ^s_{ijk}\Big] + \theta H^s_{ij(k+2)} \\
H^s_{(i+1)j(k+2)} =& \frac{\alpha}{k}\Big[H_{ijk} + j\delta H^s_{i(j-1)k} + i\alpha H^s_{(i-1)jk} - sJ^s_{ijk}\Big] + \gamma H^s_{ij(k+2)} \\
H^r_{i(j+1)(k+2)} =& \frac{\delta}{k}\Big[H_{ijk} + j\delta H^r_{i(j-1)k} + i\alpha H^r_{(i-1)jk} - rJ^s_{ijk}\Big] + \theta H^r_{ij(k+2)} \\
H^r_{(i+1)j(k+2)} =& \frac{\alpha}{k}\Big[H_{ijk} + j\delta H^r_{i(j-1)k} + i\alpha H^r_{(i-1)jk} - rJ^s_{ijk}\Big] + \gamma H^r_{ij(k+2)} \\
H_{(i+1)jk} =& \alpha(H^s_{ijk} + H^r_{ijk}) + \gamma H_{ijk} \\
H_{i(j+1)k} =& \delta(H^s_{ijk} + H^r_{ijk}) + \theta H_{ijk} \\
H_{ij(k+2)} =& \frac{1}{kd^2(1-c^2)}\Big[(\boldsymbol{R}\cdot\boldsymbol{t})J^s_{ijk} + i\gamma H_{(i-1)jk} + j\theta H_{i(j-1)k} - (2+i+j-k)H_{ijk}\Big]
\end{aligned}$$

A.3 Special case of collinear segments

When two dislocation segments are collinear and do not intersect, the distance between them reduces to $\boldsymbol{R} = (r+s)\boldsymbol{t}$ and the integrals H, H^s and H^r can be computed explicitly. There are given for $i+j = k-2$ by

$$\begin{aligned}
H &= (\boldsymbol{t}\cdot\boldsymbol{e_{12}})^i(\boldsymbol{t}\cdot\boldsymbol{e_3})^j \int\int \frac{(r+s)^k}{|r+s|^{k+2}} dsdr = -\alpha^i\delta^j\frac{(r+s)^{k-1}}{|r+s|^k} \\
H^s &= (\boldsymbol{t}\cdot\boldsymbol{e_{12}})^i(\boldsymbol{t}\cdot\boldsymbol{e_3})^j \int\int \frac{(r+s)^k}{|r+s|^{k+2}} sdsdr = -\alpha^i\delta^j r\frac{(r+s)^k}{|r+s|^k}\ln(r+s).
\end{aligned}$$

The stress at a point $\boldsymbol{x}$ coming from a segment $[\boldsymbol{x_1}, \boldsymbol{x_2}]$ that does not contain $\boldsymbol{x}$, Eq. (12) is

$$\sigma_{js} \approx \epsilon_{ngr} C_{jsvg} C_{pdwn} b'_w t'_r \sum_{q=0}^{q_{\max}} \sum_{m=0}^{2q+1} \Re \left(S^{qm}_{vpd} J^r_{m,(2q+1-m),2q+3} \right)$$

where J^r is defined in Eq. (A.2) and expressed using recurrence relations in Eqs. (A.3-A.4). The distance between $\boldsymbol{x}$ and the segment is $\boldsymbol{R} = r\boldsymbol{t'} + d\boldsymbol{u}$ with $\boldsymbol{u} = \boldsymbol{R} - (\boldsymbol{R} \cdot \boldsymbol{t'})\boldsymbol{t'}$ and $d = \frac{\boldsymbol{R} \cdot \boldsymbol{u}}{\boldsymbol{u} \cdot \boldsymbol{u}}$.

In the collinear case, where $\boldsymbol{R} = r\boldsymbol{t'}$ and $\boldsymbol{x}$ does not intersect the dislocation segment $[\boldsymbol{x_1}, \boldsymbol{x_2}]$, the single integral J^r can be computed explicitly and is given for $i + j = k - 2$ by

$$J^r = (\boldsymbol{t'} \cdot \boldsymbol{e_{12}})^i (\boldsymbol{t'} \cdot \boldsymbol{e_3})^j \int \frac{r^k}{|r|^{k+2}} dr = -\beta^i \epsilon^j \frac{r^{k-1}}{|r|^k}.$$

Acknowledgments

Lawrence Livermore National Laboratory is operated by Lawrence Livermore National Security, LLC, for the U.S. Department of Energy, National Nuclear Security Administration under Contract DE-AC52-07NA27344.

References

[1] S. P. Fitzgerald and S. Aubry. Self-force on dislocation segments in anisotropic crystals. *Journal of Physics: Condensed Matter*, 22(29):295403, 2010.

[2] S. Aubry, S. Fitzgerald, S. Dudarev, and W. Cai. Equilibrium shapes of dislocation shear loops in anisotropic alpha-fe. *Modelling and Simulation in Materials Science and Engineering*, 19:065006, 2011.

[3] S.P. Fitzgerald and Z. Yao. Shape of prismatic dislocation loops in anisotropic α-Fe. *Philosophical Magazine Letters*, 89(9):581–588, 2009.

[4] S. Fitzgerald, S. Aubry, S. Dudarev, and W. Cai. Discrete dislocation dynamics simulation of frank-read sources in anisotropic alpha-fe. *Modelling and Simulation in Materials Science and Engineering*, 2012.

[5] M. Rhee, J. S. Stolken, V. V. Bulatov, T. Diaz de la Rubia, H. M. Zbib, and J. P. Hirth. Dislocation stress fields for dynamic codes using

anisotropic elasticity: methodology and analysis. *MSMSE*, A309-310:288–293, 2001.

[6] W. Puschl. Reactions between glide dislocations and forest dislocations in anisotropic bcc crystals. *Phys. Stat. Sol. A*, 181, 1985.

[7] X. Han, N. M. Ghoniem, and Z. Wang. Parametric dislocation dynamics of anisotropic crystals. *Phil. Mag.*, 83(31-34, SI):3705–3721, 2003.

[8] J.P. Hirth and J. Lothe. *Theory of Dislocations.* Krieger publishing company, 1982.

[9] J. Yin, D. M. Barnett, and W. Cai. Efficient computation of forces on dislocation segments in anisotropic elasticity. *MSMSE*, 18(045013), 2010.

[10] A Arsenlis, W Cai, M Tang, M Rhee, T Oppelstrup, G Hommes, T G Pierce, and V V Bulatov. Enabling strain hardening simulations with dislocation dynamics. *Modelling and Simulation in Materials Science and Engineering*, 15(6):553–595, 2007.

[11] T. Mura and N. Kinoshita. Green's functions for anisotropic elasticity. *Phys. Stat. Sol. (b)*, 47:607, 1971.

[12] D.J. Bacon, D.M. Barnett, and R.O. Scattergood. Anisotropic continuum theory of lattice defects. *Prog. Mater. Sci.*, 23:51–262, 1980.

[13] D. M. Barnett. The precise evaluation of derivatives of the anisotropic elastic green's functions. *physica status solidi (b)*, 49(2):741–748, 1972.

[14] M. Abramowitz and I.A. Stegun. *Handbook of Mathematical Functions: With Formulas, Graphs, and Mathematical Tables : [is an Outgrowth of a Conference on Mathematical Tables Held at Cambridge, Mass., on 1954.* Applied mathematics series. Dover Publ., 1965.

[15] Vasily Bulatov, Wei Cai, Jeff Fier, Masato Hiratani, Gregg Hommes, Tim Pierce, Meijie Tang, Moono Rhee, Kim Yates, and Tom Arsenlis. Scalable line dynamics in paradis. In *Proceedings of the 2004 ACM/IEEE conference on Supercomputing*, SC '04, pages 19–, Washington, DC, USA, 2004. IEEE Computer Society.